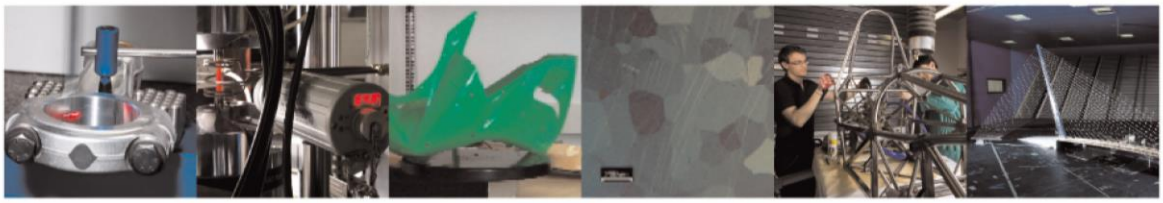

Additive manufacturing of laser cutting nozzles by SLM: processing, finishing and functional characterization

Anilli, Marco; Demir, A. G.; Previtali, B.

DIPARTIMENTO DI MECCANICA ■ POLITECNICO DI MILANO
via G. La Masa, 1 ■ 20156 Milano ■ EMAIL (PEC): pecmecc@cert.polimi.it
http://www.mecc.polimi.it
Rev. 0

Additive manufacturing of laser cutting nozzles by SLM: Processing, finishing and functional characterization

Marco Anilli[1], Ali Gökhan Demir[1]*, Barbara Previtali[1],

[1]Department of Mechanical Engineering, Politecnico di Milano, Via La Masa 1, 20156 Milan, Italy

*Corresponding author; aligokhan.demir@polimi.it

Abstract

Purpose –This work demonstrates the use of selective laser melting for producing single and double chamber laser cutting nozzles. The main aim is to assess a whole production chain composed of an additive manufacturing (AM) and consecutive finishing processes together. Beyond the metrological and flow related characterization of the produced nozzles, functional analysis on the use of the produced nozzles are carried out through laser cutting experiments.

Design/methodology/approach – SLM experiments were carried out to determine the correct compensation factor to achieve a desired nozzle diameter on steel with known processability by SLM and using standard nozzle geometries for comparative purposes. The produced nozzles are finished through electrochemical machining (ECM) and abrasive flow machining (AFM). The performance of nozzles produced via additive manufacturing (AM) are compared to conventional ones on an industrial laser cutting system through cutting experiments with a 6 kW fiber laser. The produced nozzles are characterized in terms of pressure drop and flow dynamics through Schlieren imaging.

Findings – The manufacturing chain was regulated to achieve 1 mm diameter nozzles after consecutive post processing. The average surface roughness could be lowered by approximately 80%. The SLM produced single chamber nozzles would perform similarly to conventional nozzles during the laser cutting of 1 mm mild steel with nitrogen. The double chamber nozzles could provide complete cuts with oxygen on 5 mm-thick mild steel only after post-processing. Post-processing operations proved to decrease the pressure drop of the nozzles. Schlieren images showed jet constriction at the nozzle outlet on the as-built nozzles.

Originality/value – In this work, the use of an additive manufacturing process is assessed together with suitable finishing and functional analysis of the related application to provide a complete production and evaluation chain. The results show how the finishing processes should be allocated in an AM based

production chain in a broader vision. In particular, the results confirm the functionality for designing more complex nozzle geometries for laser cutting, exploiting the flexibility of SLM process.

Keywords: Selective laser melting; electrochemical machining; abrasive flow machining; surface finishing; Schlieren

Paper type: Research paper

Nomenclature

ACRONYM OR SYMBOL	PARAMETER	UNIT
bc	Beam Compensation	µm
%ΔP	Percentage Pressure drop	
D_{cad}	CAD Diameter	mm
d_h	Hatch Distance	µm
d_p	Point Distance	µm
D_{SLM}	SLM Diameter	mm
P	Laser Power	kW
P_{com}	Commanded Pressure	bar
P_{meas}	Measured Pressure	bar
R_a	Average arithmetic Roughness	mm
RONt	Total Roundness	mm
s.o.d.	Stand-off Distance	mm
W_t	Total Waviness	µm
z	Layer Thickness	µm
ϑ	Orientation	°

1. Introduction

Selective laser melting (SLM) is an industrially accepted additive manufacturing technique based on powder bed fusion for producing metallic components (Lee et al., 2017). One of the key features that provided such acceptance is the possibility for generating lightweight structures (Yan et al., 2012),(Yan et al., 2014), complex shapes (Petrovic et al., 2011), and internal channels (Armillotta et al., 2014). In terms of the internal channel generation, the SLM process provides the means for avoiding assembly and design of conformal designs (Mazur et al., 2016). The advantage of producing internal and conformal channels comes along with the problems associated to their dimensioning, tolerancing (Ameta et al., 2015), and inspection (Pakkanen et al., 2016). It has been shown that the accuracy of a simple circular hole produced by SLM can depend on its dimension (Kempen et al., 2014) and build orientation (Morgan et al., 2016)(Snyder et al., 2015a). It has

been observed that horizontal holes are not easy to produce without the use of support structures. Horizontal holes are defected around the upper surface of the hole, where the surface inclination goes above 45°. The geometrical defect is amplified for larger holes. As a common solution, support structures are generated along the hole, which are later on removed by subtractive processes. Such solution is not applicable for small diameter channels running conformal to the part geometry.

Another important issue is the surface roughness of the SLM produced parts. The outer surface of the SLM produced components are characterized by high surface roughness (Ra=5-15 μm) (Strano et al., 2013). Surface roughness depends on several factors ranging from the process parameters (Król et al., 2013) to the part inclination (Strano et al., 2013) and used powder size (Spierings et al., 2010). Concerning internal channels, a further difficulty exists in terms of inspection and measurement of the surface roughness. The use of computed tomography is a possible solution for reconstructing the internal channel geometry (Snyder et al., 2015b), which is limited to the inspectable material thickness, resolution and available source power. The use of destructive inspection techniques remains applicable as a means to identify the process capability in simpler geometries of small products.

The fact that these internal channels are difficult to reach for post-processing operations and their surface quality is hard to improve is an important industrial challenge. Despite evident issue, the post-processing methods regarding the finishing of internal channels produced by SLM has received very little attention from the research communities. Some researchers have investigated the use of different surface finishing techniques over the external surfaces of the SLM produced parts. Mechanical methods such as grinding and sandblasting are usually applicable to only outer surfaces, and can reduce the average surface roughness between 0.3-2 μm depending on the grit size (Löber et al., 2013). Concerning internal channels, methods based on a liquid or flow medium that can pass through the internal channels can provide the means for reaching through the internal channels. Such methods usually rely on chemical or electrochemical dissolution or plasma erosion (Löber et al., 2013),(Lyczkowska et al., 2014). The electrochemical and plasma polishing methods are usually applied with universal electrodes or tools, which are fit for improving the outer surface quality. The efficacy of the process can be improved by the use of dedicated tools matching the form of the channel. The results of the recent research show that the combined use of different techniques

are most effective for reducing the surface roughness (Löber et al., 2013). Moreover, an evident interaction exists between the initial and final surface conditions, underlining the importance of the surface condition obtained after the SLM process (Demir and Previtali, 2017a). The SLM process also lends itself for in-process improvement of the surface quality, where surface remelting has been shown to be successful to limited extent (Kruth et al., 2008) (Demir and Previtali, 2017b). The use laser ablation (Yasa and Kruth, 2010) and also hybrid manufacturing with the use of integrated milling systems ("Sodick Co Ltd, OPM350L," n.d.),("MC Machinery Systems Inc, Lumex Avance 25," n.d.) between consecutive layers are other possibilities that require further attention.

The basic research reported in the literature provides benchmark values for the improvements achievable via different finishing operations and geometrical tolerances achievable for internal channels. The planning of both additive manufacturing and post-processing phases from the point view of a given application appears to be largely neglected in literature. The cycle of product manufacture should be also evaluated through functional testing of the product in addition to the standard quality metrics. Accordingly, this paper studies the use of SLM and post-processing techniques to manufacture laser cutting nozzles. Laser cutting nozzles are fundamental components for the laser cutting process providing either an inert (e.g. N_2 and Ar) or reactive (O_2) gas. The process gas can provide either protection from oxidation or induce it for providing oxidation enthalpy (Steen and Mazumder, 2010). Moreover, the gas exerts pressure over the molten metal pushing it outside the open kerf, which provides the separation mechanism. In the recent years, the use of non-symmetrical nozzles has gained attention, which can improve the laser cutting performance in terms of cut kerf quality (Rodrigues et al., 2017). Such nozzles are difficult to produce by conventional techniques and may require the assembly of multiple parts. Thus, this work provides the basis comparison between SLM produced, post-processed, and conventional nozzles. In the initial part of the work SLM and post-processing phase composed of electrochemical machining (ECM) and abrasive flow machining (AFM) are investigated together. The produced nozzles are then extensively characterized in terms of surface roughness and nozzle outlet roundness improvement. Functional tests in terms of flow characteristics and laser cutting experiments are provided. Figure 1 summarizes the main stages of the work.

Figure 1. Scheme of the main steps of the work.

2. Materials and methods

2.1. Material

The metal powder used in this work is 18Ni300 maraging steel (Sandvik Osprey, Neath, UK), which composition is reported in Table 1 and a scanning electron microscope (SEM) image of the powder is provided in Figure 2-a. The powder is obtained by gas atomization with nitrogen. The powder is spherical in shape and with size distribution following D10 at 20 μm, D50 at 32 μm, and D90 at 54 μm. Powder flowability was measured at 14.2 s/50g. The curve of the particle size distribution is shown in Figure 2-b. The material is suited for tooling applications. It was preferred at this stage of feasibility investigation due to its known processability via SLM (Demir et al., 2017). Conventional nozzles are produced in Cu-alloys, which are not commonly used in SLM due to their high reflectivity. Electron beam melting has been demonstrated to be effective for additive manufacturing of Cu-based alloys (Ramirez et al., 2011). However, the feature resolution of EBM is lower than that of SLM, which is the main limitation for producing small internal channels required for the application. On the other hand, the SLM process for Cu is being developed by the use of high power fiber lasers (Ikeshoji et al., 2017). Currently, the main issue remains as the high porosity (approximately 4%). The material choice for conventional nozzles reflects the preference for improved heat conductivity around the nozzle to avoid heat accumulation in prolonged uses. This was not an issue in the present work.

Table 1. Chemical composition of 18Ni300 maraging steel.

Figure 2. SEM image of 18Ni300 steel powder (1000x magnification) (a) and powder size distribution curve (b).

2.2. Nozzle geometries

The geometry of the laser cutting nozzles is shown in Figure 3. Two models of nozzles have been considered: a conical-convergent single chamber and the corresponding double chamber version, both in 1 mm size. The single chamber design is employed for laser cutting of thin sheet metal (1 mm-thick) with N_2 assist gas. The double chamber design is used for cutting thicker sheets (≥5 mm). Within the experimental work both designs were produced by SLM, and compared to the conventional nozzle in Cu-alloy. Conventional nozzles made in Cu-based alloy and have an inner roughness R_a lower than 0.40 μm. The

nozzle diameter tolerance was given as 1 ± 0.02 mm, whereas the roundness of the conventional nozzles was measured at 0.005 ± 0.001 mm. In Figure 3 the main dimensional specifications of the nozzles are reported, Figure 4 shows three axial sections of a double chamber nozzle in three different conditions (SLM as-built (a), post-processed (b), standard nozzle (c)) and Figure 5 provides a view of 90° and 45° oriented nozzles on the substrate.

Figure 3. Axial sections of a conical-convergent single chamber nozzle (a) and the corresponding double chamber version (b), both in 1 mm size.

Figure 4. Axial sections of a double chamber nozzle in three conditions: SLM as-built (a), SLM post-processed (b) and standard (c).

Figure 5. Side view of a nozzle printed with a 90° (a) and 45° (b) orientation. Supporting structures can also be observed.

2.3. Selective laser melting (SLM) system

The SLM system employed in this work is a Renishaw AM250 machine (Stone, UK). The maximum building volume is 245 x 245 x 300 mm^3, handling up to 40 nozzles produced within a single build. The system is equipped with a 200 W single mode active fiber laser (SPI R4, Southampton, UK), which operates in pulsed wave emission by power modulation. The laser beam is focused at the powder surface, with a spot size of 75 μm. Processing is carried out under Ar, and a circulation pump maintains the gas flow parallel to the powder bed and the oxygen content of the process chamber is maintained below 1000 ppm.

2.4. Electrochemical machining (ECM) system

ECM was used to improve the surface quality of the conical upper section of the nozzles. The process is based on an anodic dissolution, where the machined part is the anode and a dedicated cathode is used. Both electrodes are immersed in an electrolyte and electrical current is applied (Bhattacharyya et al., 2004). The process is schematically described in Figure 6. A dedicated cathode is used with a conformal form of the conical section of the nozzle chamber. Hence, the cylindrical tip could not be processed. An industrial ECM system was employed (Extrude Hone Coolpulse). The electrolyte is denominated ES-G 8020 and is stored in an isolated PE tank, with a maximum capacity of 850 l. The system provides temperature control as well as the filtering of the solution. The filtration unit is constituted by a chamber filter press with 15 filters and the maximum filtration capacity is 5 l at filter surface area (5 m^2). The electrical connected load is 35 kVA/s, 500 A current with a 30 V voltage. Figure 7 shows the details of the process.

Figure 6. Stages of the finishing of the SLM produced nozzles.

Figure 7. Details of the ECM process applied to the SLM produced nozzles.

2.5. Abrasive flow machining (AFM) system

As the second finishing step AFM was used. In particular, AFM was used to improve the surface quality of the cylindrical tip. In AFM an abrasive medium, commonly a carbide, and a polymeric carrier is used, which is pushed through the machined zone through the use of hydraulic system (Kumar and Hiremath, 2016). The process allowed for reaching thinner sections of the channels and provided roughness reduction by abrasion. An industrial AFM system was employed (Extrude Hone EcoFlow). The abrasive media system is constituted by a 80 x 250 mm^2 (diameter x stroke length) cylinder, with a maximum capacity of 1.3 dm^3 and capable of exert a pressure range from 3.4 to 20.7 MPa. The abrasive media flow rate is constant and equal to 4.1 dm^3/min. The abrasive medium is commercially denominated 831/150s and contains SiC abrasive particles (mesh 150). AFM was able to reach the effective processing pressure at the nozzle tip, hence was found to be an adequate solution for improving the quality of the nozzle tip. Figure 8 shows the details of the process.

Figure 8. Details of the AFM process applied to the SLM produced nozzles.

2.6. Laser cutting and flow diagnosis setup

Cutting performance and flow diagnosis have been carried out on a laser cutting machine, that integrates a plate and a tube cutting system (BLM Group LC5). The machine is equipped with a 6 kW active fiber laser (IPG Photonics), with a 100 μm fiber, and a cutting head encasing a 100 mm collimation, 200 mm focal lenses (Precitec ProCutter). Flow diagnosis has been carried out with a digital pressure detector directly installed on the laser cutting system, capable of measuring a maximum pressure of 40 bar and featured by a precision of ±0.25%. The gas flow out of the nozzles was visualized with a Schlieren imaging system. Schlieren imaging is based on the imaging of gas discontinuities employing a light source, which is transmitted through the gas flow and imaged on a sensor (Callies et al., 1995). The discontinuities investigated in this study are due to the refractive index variations due to pressure variations induced by shock waves and similar flow discontinuities. As shown in the scheme of Figure 9, the optical chain is constituted by six linear segments and the light source is a white LED. A Barlow lens with a focal length of

45 mm focalizes the light on a CCD camera (Point Grey GS3-U3-28S4M-C), after the filtering of the light rays by the edge of a razor blade, at the end of the light path.

Figure 9. Scheme of the Schlieren apparatus. Red arrows represent the light path, that crosses the gas jet perpendicularly.

2.7. Characterization

Images of the nozzle aperture was made by a vision measurement system (Mitutoyo QV-ELF202). The working area is illuminated by halogen lamps and the images are captured by a CCD camera. The accuracy is (2+3L/1000 μm) along X and Y and (4+5L/1000 μm) along Z. Roughness of the nozzle chambers have been measured with the contact profilograph (Mahr PGK PCMESS 7024357 Perthometer Concept). The contact tip had a 5 μm tip radius.

3. Experimental plan

The experimental work consisted in three different phases.

i) Study of SLM processing conditions for producing single and double-chamber nozzles. The nozzles were built with two different orientations. Conditions that minimized surface roughness and roundness, which provided desired diameters were sought.

ii) Finishing of the produced nozzles. Identification of the improvement in the surface roughness and nozzle diameter roundness.

iii) Characterization of the nozzle performance by functional tests. Identification of pressure losses and cutting capacity of the nozzles.

Throughout the experimental work, the SLM produced nozzles were compared to the conventional ones in terms of geometry, flow characteristics, and in terms of cut quality.

3.1. Control of nozzle geometry in SLM

The aim of this phase was to produce single and double chamber nozzles with correct geometrical features. The main objective was to obtain controlled nozzle outlet diameters, minimize the inner surface roughness and the roundness value with two build orientations. In SLM, the process parameters have a direct impact on

several aspects related to surface quality and geometrical accuracy. But more importantly they determine the part density. Use of different scan strategies, remelting passes are also viable to improve surface quality. However, the present application requires surface roughness levels (Ra<1 μm) not achievable through such options. On the other hand, part dimensions on the CAD model and part orientation are strictly related to the part geometry. Accordingly, in this study process parameters were fixed enabling fully dense components were used. A statistical regression model was sought in order to control the nozzle diameter as a function of the diameter given by the CAD model (D_{cad}). Four different nozzle diameters from 0.5 to 1.25 mm were tested. The diameter of the produced nozzles was measured (D_{slm}). Part orientation was evaluated at 0° with the nozzle tip facing upwards and the nozzle inlet facing the substrate plate and 45° inclination with respect to the substrate plane. The 45° inclination was found to be suitable in order to reduce the support use. Both single and double-chamber designs were produced. Nozzle outlet roundness was evaluated as well as the average surface roughness of the chamber. Roundness is defined as:

$$RONt = R_1 - R_2 \quad (1)$$

where R_1 and R_2 are the radiuses of the minimum circumscribed and maximum inscribed circumference to the cloud of sampled points respectively, as shown in Figure 10.

Figure 10. Schematic representation for RONt index calculation. Red points represent the cloud of experimental points sampled along the hole's profile by the measuring instrument. R_1 and R_2 are the radiuses of the minimum circumscribed and the maximum inscribed circumferences respectively.

SLM parameters were fixed operating with recommended set of parameters by the system manufacturer. The maximum laser power at 200 W and pulse duration at 80 μs. Distance between consecutive laser pulses was 65 μm, whereas the distance between consecutive hatch lines was 70 μm. Beam compensation was fixed at 80 μm outside the scan contour. Throughout the work the statistical significance level was fixed at α=5%. Table 2 shows the experimental plan.

Table 2. Fixed and varied parameters in the control of nozzle geometry in SLM.

3.2. Finishing of SLM produced nozzles

The finishing of the inner surfaces of the SLM produced nozzles have been carried out applying the ECM and AFM processes in series, as shown in Figure 6. Table 3 collects the process parameters for both the stages, which are based on preliminary tests not reported here for brevity.

Table 3. Process parameters of the finishing of the SLM produced nozzles

3.3. Flow diagnosis and laser cutting experiments

Flow diagnosis have been carried out to characterize the gas jet exiting the nozzles from two points of view. First, the pressure drop at the nozzle's outlet (%ΔP) was evaluated. The pressure level commanded by the laser cutting system (P_{com}) was varied between 5 and 20 bar. Stand-off distance (s.o.d.) between the nozzle tip and the sensor, which is an important parameter in laser cutting, was varied between 0.3 and 0.7 mm. Standard nozzles were compared to those produced by SLM in as-built conditions and after post processing. All nozzles had 1 mm outlet diameter. Hence, the as-built SLM nozzles were produced with a 1 mm diameter, whereas the post-processed nozzles were initially 0.5 mm in diameter, which were enlarged to 1 mm by the post-processing steps. Pressure drop was calculated according to Equation (2) and visual analysis of the structure of the flow through Schlieren imaging. Cutting performances have been evaluated in terms of quality of the cut edges through roughness measurements. Square shaped samples with 50 mm edge length were cut with 6 kW laser power and 35000 mm/min cutting speed for 1 mm thick plates and 4000 mm/min for 5 mm. On each sample, a linear track has been measured on two corresponding different straight sides. Table 4 shows the parameters considered for this experimental campaign.

Table 4. Parameters for the flow diagnosis and laser cutting experiments.

$$\%\Delta P = \frac{P_{com} - P_{measured}}{P_{com}} \cdot 100 \qquad (2)$$

4. Results

4.1. Nozzle diameter, roundness and inner surface roughness after SLM

The statistical analysis showed no influence of the nozzle type (single or double chamber) on the nozzle diameter. Instead, the build orientation was found to be effective on the diameter variation. Figure 11-a and Figure 11-b show the plot of the regression line for ϑ=45° and ϑ=90° respectively. Equations (3) and (4) are the regression equations associated to the two different values of orientation. The regression coefficients show that with 45° part orientation, the nozzle diameter is slightly larger. There is only a slight deviation between the diameter given by the CAD model and the produced one, which shows the adequacy of the recommended beam compensation with the used process parameters. As seen in the figures, the model fits the data very well as also shown by the very high value of R^2_{adj}.

Figure 11. Fitted line plot for the regression model of CAD and actual measured diameter. a) ϑ=45°, b) ϑ=90°.

(ϑ=90°) $$D_{slm} = -0.0252 + 0.9984 D_{cad}$$ (3)

(ϑ=45°) $$D_{slm} = -0.0938 + 0.9984 D_{cad}$$ (4)

Analysis of variance (ANOVA) was applied to the roundness measurements. The resultant ANOVA table is shown in Table 5. The only statistically significant parameter is the orientation. As seen in Figure 12, part orientation at 45° results in an oval outlet profile. As reported in Figure 13-a nozzle tip the hole axis parallel to the build direction (90°) provides a decrease of 30% in roundness value compared to the part orientation used for reducing the support use (45°).

Table 5. ANOVA table for the roundness of the holes of the SLM produced nozzles.

Figure 12. Profiles of nozzle outlets built with a 90° and 45° orientation.

Figure 13. Bar chart of roundness (RONt) (a) and inner surface roughness R_a (b) of the SLM nozzles holes against the only significant factor from the ANOVA (Orientation). Error bars are one standard deviation from the mean.

Figure 14. Schematic representation showing the effect of hole inclination with respect to the build direction.

The average surface roughness of the nozzle channel showed similar results with the roundness. The results of ANOVA is shown in Table 6. Again, according to ANOVA, orientation is the only influential factor and, on the average, the value of R_a associated to ϑ=90° is lower than the one associated to 45°, as shown in Figure 13-b. The difficulty in maintaining hole accuracy in SLM is well-known for non-vertical build orientations. The deviations are more marked for larger dimensions, where the hole shape can deviate from circular to a tear shaped one around to overhang regions for horizontally oriented holes. As shown in Figure 14, when the axis of the hole is not parallel to the build direction, a small portion of the scanned layer generates an overhang region suspended on the powder bed. Such regions are more susceptible to increased surface roughness, which can also increase the geometrical error of small sized features such as the nozzle tip. The results reported here show the relevance of the orientation choice as required by the precision of the application.

Table 6. ANOVA table for the inner roughness of the SLM produced nozzles.

The results provided the choice over the build orientation as 90° was found to be more suitable for maintaining geometrical accuracy. On the other hand, the nozzle design in terms of chamber number did not affect the nozzle tip dimensions. For further investigations, both nozzle designs were produced with 0.5 mm and 1.00 mm nozzle tip diameter. The nozzle diameter on the CAD model was adjusted using the equations (3) and (4) to achieve the desired dimensions by the SLM process. The nozzles with 0.5 mm diameter were further processed with the post-processing steps.

4.2. Roughness diameter, and roundness variation after post-processing

Figure 15 shows the holes' diameter (a) and roundness (b) variation after post-processing. Figure 16 depicts the variation the inner surface roughness. Referring to Figure 15-a, it is possible to notice how the use of the regression model and the choice of the process parameters for the post-process allow to have a good control on the size of the holes. This is confirmed also by the very narrow interval of variance. In addition, the red dotted lines in the chart represent the tolerance limitations for the 1 mm holes. Both the as-built and post-processed nozzles respect this limitation. With regard to roundness, in the chart of Figure 15-b a reduction of about one order of magnitude on the mean can be observed on the holes' roundness of the SLM produced nozzles after post-processing, with respect to the as-built condition. Dealing with roughness, in Figure 16 a substantial reduction of R_a can be observed. On average, a decrease of about 85% between the as-built and the post-processed condition has been observed.

ANOVA was applied on the average surface roughness comparing the two nozzle designs and three processing conditions comparing standard nozzles with as-built and post-processed SLM nozzles. As reported in Table 7 the chamber number does not influence the final result, whereas the processing condition is the only statistically significant parameter.

Figure 15. Nozzle hole's diameter (a) and roundness (RONt) (b) variation after the post-processing of the inner surface. Error bars are one standard error from the mean.

Figure 16. Inner surface roughness R_a variation between as-built and post-processed condition. Error bars are one standard error from the mean.

Table 7. ANOVA table for the inner surface R_a after post-processing.

In conclusion to this paragraph, the colour maps associated to the surface roughness R_a before and after the post-process are provided in Figure 17. The maps are distinguished between by working area of the ECM, used to finish the upper conical section of the nozzles, and of the AFM, used in the final cylindrical channel.

Figure 17. Colour maps of the inner surface morphology of the SLM nozzles, distinguished by condition and region: upper conical section (a) and cylindrical final channel (c) in as-built quality and the corresponding finishing after ECM (b) and AFM (d).

4.3. Comparative analysis of standard, SLM produced and finished nozzles

4.3.1. Pressure drop

The results of the pressure drops evaluation are here presented separately for the two selected kind of nozzles, distinguishing between single and double chamber, but the behaviour from this point of view is very similar among them. Figure 18 show the bar chart for this set of experimental tests, distinguishing between single (a) and double (b) chamber nozzles. For both the cases, it can be observed that the pressure drop increases as the stand-off distance (s.o.d.) increases and that the condition of the inner surface of a nozzle has an impact on the response. Table 8 and Table 9 report the ANOVA results on the pressure drop for single and double chamber configurations respectively. It can be seen that s.o.d. and condition are the two most influential factors on the response and, in particular, the pressure drop associated to the as-built nozzles are the highest. On average the pressure drop of an as-built SLM nozzle is twice that of the standard nozzle. The post-processing conditions, provide notable improvements as results are comparable overall with the conventional nozzle in single chamber configuration. The post-processed double-chamber nozzle appears to outperform the standard nozzles' performance at low stand-off distances.

Figure 18. Bar chart of the pressure drop (%ΔP) for single (a) and double (b) chamber nozzles against Condition, s.o.d. and P_{com}. Error bars are one standard error from the mean.

Table 8. ANOVA table for the pressure drop (%ΔP) of single chamber nozzles.

Table 9. ANOVA table for the pressure drop (%ΔP) of double chamber nozzles.

4.3.2. Laser cutting performance

The laser cutting performance study establishes a benchmark between the different nozzles produced following conventional and additive routes. In terms of the most fundamental criteria, the cutting capacity was evaluated in terms of successful attempts over 5 cutting trials under as-built and post-processed configurations. All attempts were carried out with separate nozzles, testing the variability of the applied

production route. Figure 19 shows an overview of the quantity of tested nozzles compared to the number of successful cuts. The remarkable result from this point of view concerns the double chamber nozzles. In as-built condition, only one out of the 5 tested nozzles was able to carry out a complete cut, while all of the post-processed workpieces completed the operation. This result does not regard the single chamber nozzles and it is a further demonstration of how the inner surface finish is influential on the practical behaviour of this kind of components.

Figure 19. Bar chart comparing the number of tested nozzles to the ones capable of cutting. The assistance gas, and therefore the cutting modality, is specified between brackets.

Focusing on the cutting quality, the results of the roughness measurements on two selected corresponding cut edges on each sample are shown by the chart in Figure 20-a for the 1 mm thick plates and Figure 20-b for the 5 mm. Figure 21 and Figure 22 show an example of a 1 mm and 5 mm cut edge from two different sides of the same sample respectively. On the chart in Figure 20-a, with reference to the as-built nozzles, a certain irregularity in the surface roughness between side 1 and side 2 can be noticed, both in the average value and in the variability of R_a. This fact is in all probability due to the severely indented profile of an SLM as-built hole's profile and, in lower measure, to the high inner surface roughness of the nozzle. The irregular profile of the hole perturbs the gas fluid-dynamics making the cutting quality dependant on the direction followed by the cutting head in the plane. Conversely, considering the post-processed nozzles the overall cutting quality becomes comparable to the one obtained with a standard nozzle and, in general, much less variable among the measured specimens. This improvement is associated to a better hole roundness, together with the lower inner surface roughness, that eliminates the directionality of the cutting quality. Considering the 5 mm thick samples, obtained with double chamber nozzles, similar results were obtained comparing the post-processed SLM nozzles and the standard ones. As shown in the cart of Figure 20-b, a similar quality of the cut edges is achievable cutting with standard and post-processed SLM nozzles and the typical low values of surface roughness, obtained when cutting with oxygen, is maintained when using the additively manufactured nozzles. The surface quality of the cut edges can be observed in Figure 22 where, apart from some oxides, a very low level of striation can be noticed.

Figure 20. Bar chart of the roughness measurement of the cut edges for the 1 mm (a) and 5 mm (b) plates, distinguished by condition of the inner surface of the nozzles and by the considered side of the sample.

Figure 21. Cut edges of a 1 mm thick plate with N_2 and single chamber nozzles from two different sides of the same sample.

Figure 22. Cut edges of a 5 mm thick plate with O_2 and double chamber nozzles from two different sides of the same sample.

4.3.3. Schlieren analysis

The laser cutting experiments put into evidence irregularity and inconsistent cut quality over the different edges of the cuts under as-built conditions. The Schlieren images help understanding the gas flow dynamics at stationary conditions. The typical structure of the gas jet exiting from the single chamber nozzles at 15 bar can be observed in Figure 23. Concerning the standard nozzle, the flow jet is constituted by an initial bell-shaped show-wave front that collapses on a transversal shock wave, separating this first part of the flow from a final columnar section. This structure, a part from slight dimensional differences, is the same for a single and a double chamber nozzle, therefore this distinction is no longer made in this paragraph. Considering the as-built nozzle shown in Figure 23, a certain constriction of the gas jet can be noticed, since the position of end of the bell-shaped front is retracted closer to the nozzle and is overall narrower. This is expected to be due fluid dynamic losses occurring near the nozzle's outlet and due to the rough inner surface and the irregular profile of the hole in as-built quality. Referring to the post processed nozzle of Figure 23, the jet recovers almost completely its natural position and size thanks to a smoother inner surface and a more regular hole's profile, even though some irregularities, especially at the base of the bell-shaped shock-wave front still remain. The qualitative analysis underlines a link between the surface quality, geometry of the additively produced nozzles and their cutting performance. At this level, the results are only analysed as a benchmark for understanding the differences between the standard component and additively produced and finished counterparts. Further modelling is required to better interpret the results and predict the desired flow behaviour.

Figure 23. Schlieren visualizations of the gas jet exiting a standard, an SLM as-built and post-processed nozzle. (15 bar commanded pressure).

5. Conclusions

This work investigated the production of laser cutting nozzles via selective laser melting and consecutive post-processing stages namely electrochemical machining and abrasive flow machining. The work aimed to

tackle the issue of evaluating the post-processing steps within a production cycle initiated with an additive manufacturing process. In particular, the functional testing of the specific product was carried out to provide a benchmark with the nozzles produced following a conventional manufacturing scheme. Following the same intention to provide a benchmark, the traditional nozzle geometries with single and double chambers were produced using a steel which is processable by SLM. The main findings of this work are as follows.

- The SLM process can be tightly controlled to achieve small diameter holes (0.5-1 mm), where the influence of part orientation should be considered both for support use and geometrical accuracy.
- With the correct use part design and build orientation, SLM produced nozzles respect the diameter tolerances given for nozzles produced through conventional turning.
- The inner surface roughness and hole roundness of the as-built SLM nozzles are significantly out of the requirements of the application. The use of a combined post-processing sequence allows for improving the roundness by 40%, whereas approximately 85% reduction in average surface roughness can be achieved.
- The functional tests show that reactive cutting with low O_2 pressure and as-built double chamber nozzles is not feasible. The complex nozzle geometry and low gas pressure combined with the poor surface quality result in non-functional nozzles.
- As-built single chamber nozzles used with high pressure N_2 appear to be more tolerant as complete cuts could be achieved at all times. However, the cuts were inconsistent in terms of edge quality.
- Post-processing improved cutting performance in all cases. Surface roughness of the cut edges was closer to that obtained with standard nozzles and was consistent around the different sides of the cut specimens.

The results overall underline the importance of the post-processing step over the functionality of the SLM produced component. This means that the manufacturing cycle should be designed considering the post-processing steps within the additive manufacturing step. The performance can be of laser cutting nozzles can be further improved by applying the geometrical flexibility of the process to new designs, considering also non-symmetrical design possibilities or multiple channels. It should be however noted that the post-

processability of the complex form should be considered within the design stage in order to ensure the functionality.

References

Ameta, G., Lipman, R., Moylan, S., Witherell, P., 2015. Investigating the Role of Geometric Dimensioning and Tolerancing in Additive Manufacturing. J. Mech. Des. 137, 111401. doi:10.1115/1.4031296

Armillotta, A., Baraggi, R., Fasoli, S., 2014. SLM tooling for die casting with conformal cooling channels. Int. J. Adv. Manuf. Technol. 71, 573–583. doi:10.1007/s00170-013-5523-7

Bhattacharyya, B., Munda, J., Malapati, M., 2004. Advancement in electrochemical micro-machining. Int. J. Mach. Tools Manuf. 44, 1577–1589. doi:10.1016/j.ijmachtools.2004.06.006

Callies, G., Berger, P., Hugel, H., 1995. Time-resolved observation of gas-dynamic discontinuities arising during excimer laser ablation and their interpretation. J. Phys. D. Appl. Phys. 28, 794–806. doi:10.1088/0022-3727/28/4/026

Demir, A.G., Colombo, P., Previtali, B., 2017. From pulsed to continuous wave emission in SLM with contemporary fiber laser sources: effect of temporal and spatial pulse overlap in part quality. Int. J. Adv. Manuf. Technol. doi:10.1007/s00170-016-9948-7

Demir, A.G., Previtali, B., 2017a. Additive manufacturing of cardiovascular CoCr stents by selective laser melting. Mater. Des. 119, 338–350. doi:10.1016/j.matdes.2017.01.091

Demir, A.G., Previtali, B., 2017b. Investigation of remelting and preheating in SLM of 18Ni300 maraging steel as corrective and preventive measures for porosity reduction. Int. J. Adv. Manuf. Technol. 1–13. doi:10.1007/s00170-017-0697-z

Ikeshoji, T.T., Nakamura, K., Yonehara, M., Imai, K., Kyogoku, H., 2017. Selective Laser Melting of Pure Copper, in: 29th Annual International Solid Freeform Fabrication Symposium - An Additive Manufacturing Conference. Austin, TX.

Kempen, K., Welkenhuyzen, F., Qian, J., Kruth, J., 2014. Dimensional accuracy of internal

channels in SLM produced parts. Proc. - ASPE 2014 Spring Top. Meet. Dimens. Accuracy Surf. Finish Addit. Manuf. 76–79.

Król, M., Dobrzański, L., Reimann, I., 2013. Surface quality in selective laser melting of metal powders. Arch. Mater. Sci. 60, 87–92.

Kruth, J.-P., Yasa, E., Deckers, J., 2008. Roughness improvement in selective laser melting. Proc. 3rd Int. Conf. Polym. Mould. Innov. 170–183.

Kumar, S.S., Hiremath, S.S., 2016. A Review on Abrasive Flow Machining (AFM). Procedia Technol. 25, 1297–1304. doi:10.1016/j.protcy.2016.08.224

Lee, J.-Y., An, J., Chua, C.K., 2017. Fundamentals and applications of 3D printing for novel materials. Appl. Mater. Today 7, 120–133. doi:10.1016/j.apmt.2017.02.004

Löber, L., Flache, C., Petters, R., Kühn, U., Eckert, J., 2013. Comparison of different post processing technologies for SLM generated 316l steel parts. Rapid Prototyp. J. 19, 173–179. doi:10.1108/13552541311312166

Lyczkowska, E., Szymczyk, P., Dybała, B., Chlebus, E., 2014. Chemical polishing of scaffolds made of Ti-6Al-7Nb alloy by additive manufacturing. Arch. Civ. Mech. Eng. 14, 586–594. doi:10.1016/j.acme.2014.03.001

Mazur, M., Leary, M., McMillan, M., Elambasseril, J., Brandt, M., 2016. SLM additive manufacture of H13 tool steel with conformal cooling and structural lattices. Rapid Prototyp. J. 22, 504–518. doi:10.1108/RPJ-06-2014-0075

MC Machinery Systems Inc, Lumex Avance 25 [WWW Document], n.d. URL https://www.mcmachinery.com/products-and-solutions/lumex-avance/ (accessed 3.2.17).

Morgan, H.D., Cherry, J.A., Jonnalaganna, S., Ewing, D., Sienz, J., 2016. Part orientation

optimisation for the additive layer manufacture of metal components. Int. J. Adv. Manuf. Technol. 1–9. doi:10.1007/s00170-015-8151-6

Pakkanen, J., Calignano, F., Trevisan, F., Lorusso, M., Ambrosio, E.P., Manfredi, D., Fino, P., 2016. Study of Internal Channel Surface Roughnesses Manufactured by Selective Laser Melting in Aluminum and Titanium Alloys. Metall. Mater. Trans. A Phys. Metall. Mater. Sci. 47, 1–8. doi:10.1007/s11661-016-3478-7

Petrovic, V., Vicente Haro Gonzalez, J., Jordá Ferrando, O., Delgado Gordillo, J., Ramón Blasco Puchades, J., Portolés Griñan, L., 2011. Additive layered manufacturing: sectors of industrial application shown through case studies. Int. J. Prod. Res. 49, 1061–1079. doi:10.1080/00207540903479786

Ramirez, D.A., Murr, L.E., Li, S.J., Tian, Y.X., Martinez, E., Martinez, J.L., Machado, B.I., Gaytan, S.M., Medina, F., Wicker, R.B., 2011. Open-cellular copper structures fabricated by additive manufacturing using electron beam melting. Mater. Sci. Eng. A 528, 5379–5386. doi:10.1016/j.msea.2011.03.053

Rodrigues, G.C., Decroos, C., Duflou, J.R., 2017. Considerations on Assist Gas Jet Optimization in Laser Cutting with Direct Diode Laser. Procedia Eng. 183, 37–44. doi:10.1016/j.proeng.2017.04.008

Snyder, J.C., Stimpson, C.K., Thole, K.A., Mongillo, D., 2015a. Build Direction Effects on Additively Manufactured Channels. Vol. 5A Heat Transf. 138, V05AT11A034. doi:10.1115/GT2015-43935

Snyder, J.C., Stimpson, C.K., Thole, K.A., Mongillo, D.J., 2015b. Build Direction Effects on Microchannel Tolerance and Surface Roughness. J. Mech. Des. 137, 111411. doi:10.1115/1.4031071

Sodick Co Ltd, OPM350L [WWW Document], n.d. URL http://www.sodick.jp/product/tool/metal_3d_printer/index.html (accessed 3.2.17).

Spierings, a B., Herres, N., Levy, G., Buchs, C., 2010. Influence of the particle size distribution on surface quality and mechanical properties in additive manufactured stainless steel parts. Solid Free. Fabr. Symp. 397–406.

Steen, W.M., Mazumder, J., 2010. Laser Material Processing, Media. Springer London, London. doi:10.1007/978-1-84996-062-5

Strano, G., Hao, L., Everson, R.M., Evans, K.E., 2013. Surface roughness analysis, modelling and prediction in selective laser melting. J. Mater. Process. Technol. 213, 589–597. doi:10.1016/j.jmatprotec.2012.11.011

Yan, C., Hao, L., Hussein, A., Raymont, D., 2012. Evaluations of cellular lattice structures manufactured using selective laser melting. Int. J. Mach. Tools Manuf. 62, 32–38. doi:10.1016/j.ijmachtools.2012.06.002

Yan, C., Hao, L., Hussein, A., Young, P., Raymont, D., 2014. Advanced lightweight 316L stainless steel cellular lattice structures fabricated via selective laser melting. Mater. Des. 55, 533–541. doi:10.1016/j.matdes.2013.10.027

Yasa, E., Kruth, J.P., 2010. Investigation of laser and process parameters for Selective Laser Erosion. Precis. Eng. 34, 101–112. doi:10.1016/j.precisioneng.2009.04.001

List of figures

List of tables

Step 1.
Optimal 3D printing strategy

- Dimensions
- Geometry
- Inner roughness

Step 2.
Inner surface finishing

- Combination of ECM and AFM

Step 3.
Functional tests

- Pressure losses
- Cutting tests
- Schlieren images

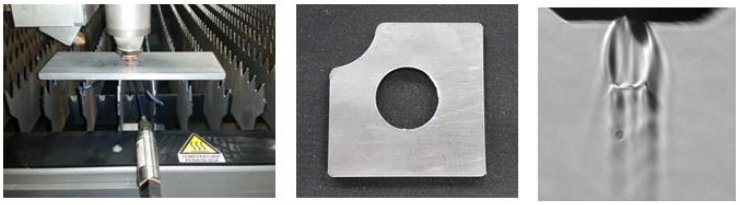

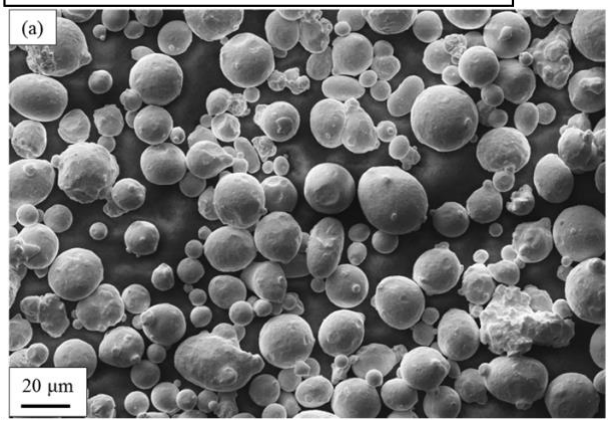

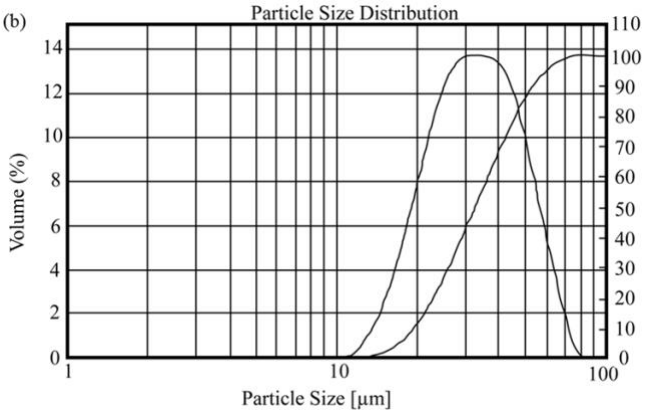

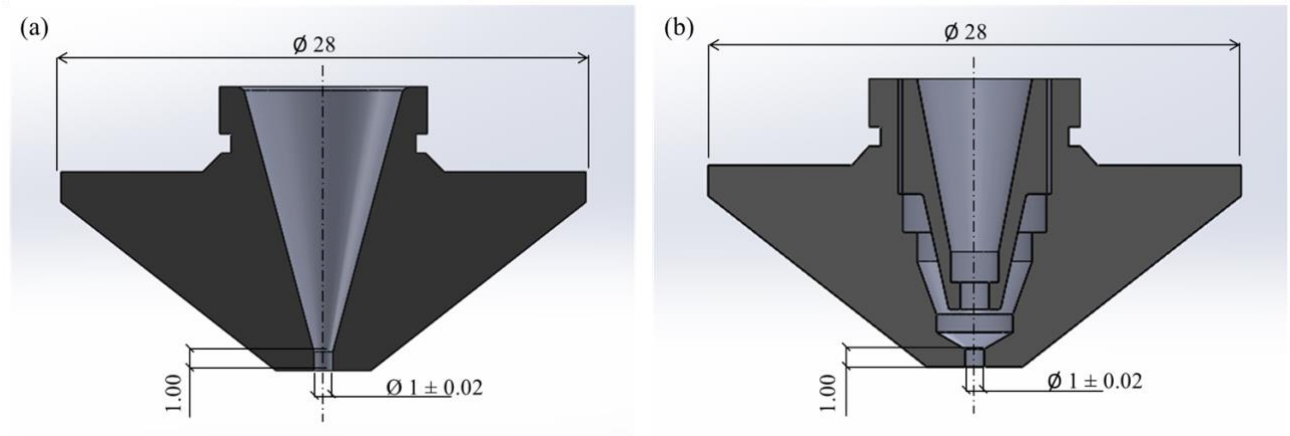
(a)
Ø 28
1.00
Ø 1 ± 0.02
(b)
Ø 28
1.00
Ø 1 ± 0.02

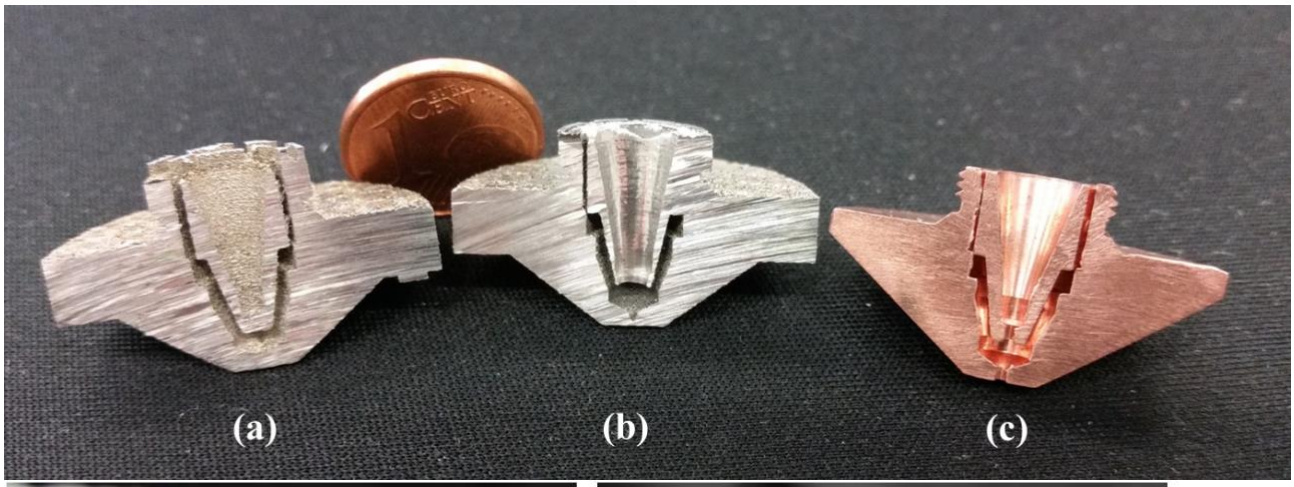
(a)
(b)
(c)

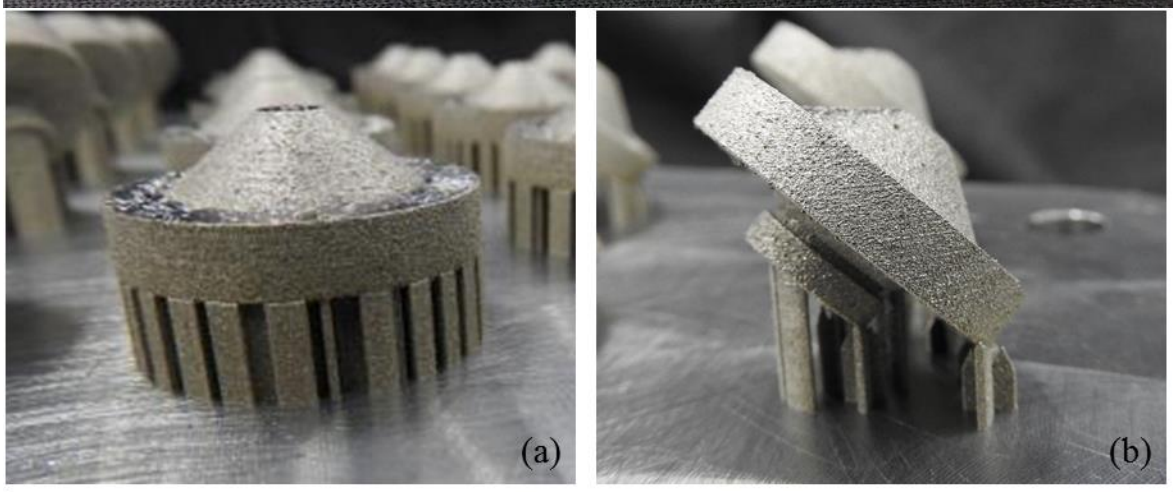
(a)
(b)

Electro-Chemical Machining (ECM)

Abrasive Flow Machining (AFM)

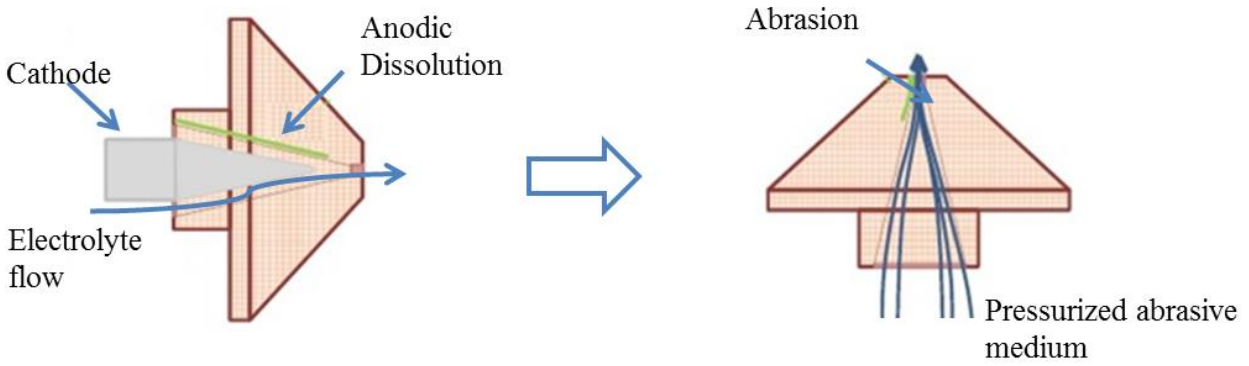

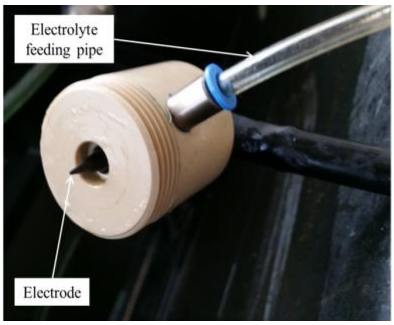

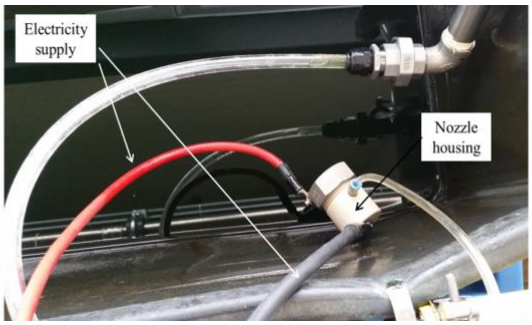

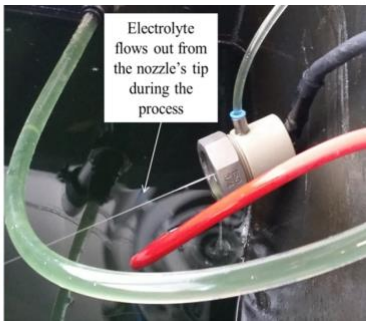

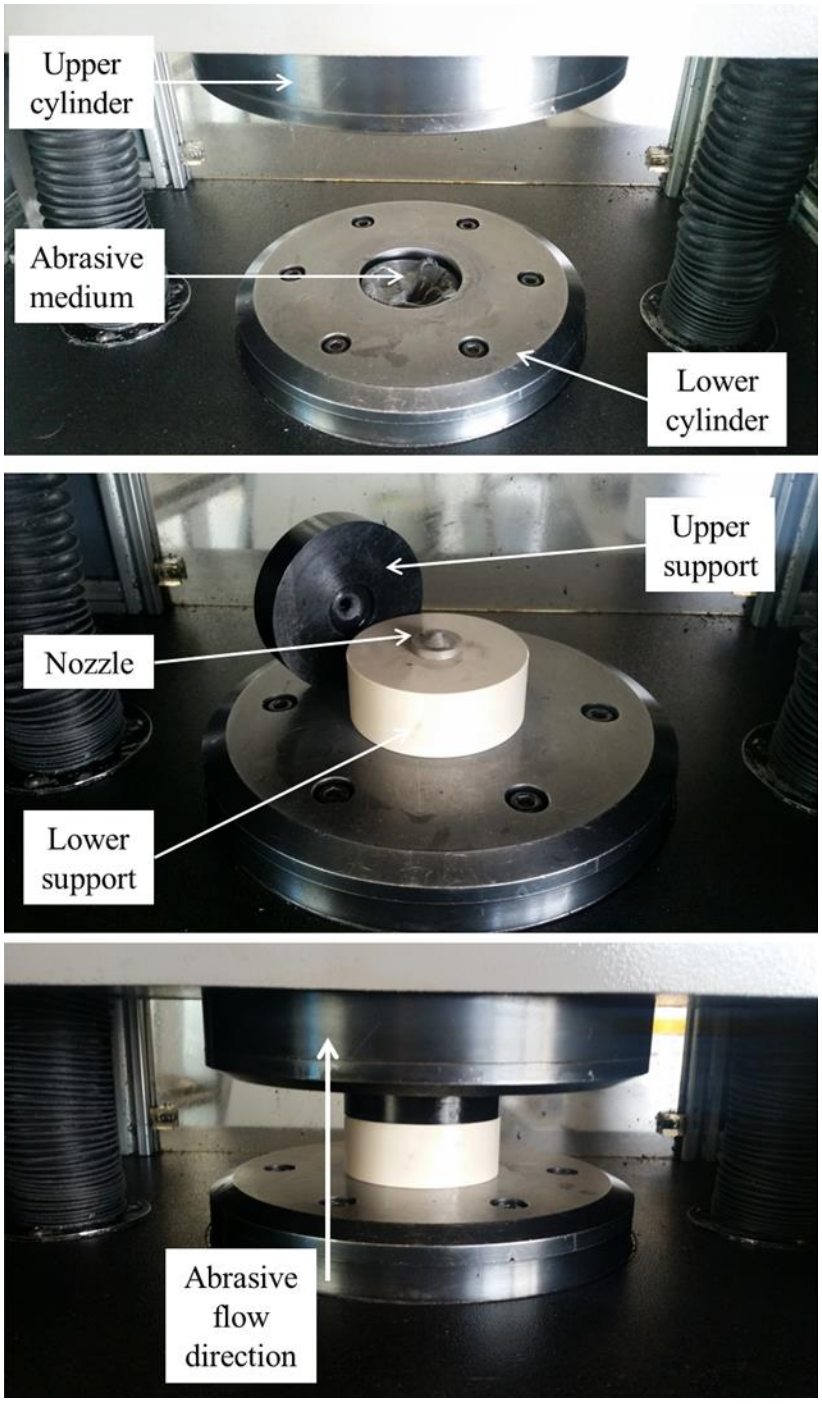
Upper cylinder
Abrasive medium
Lower cylinder
Upper support
Nozzle
Lower support
Abrasive flow direction

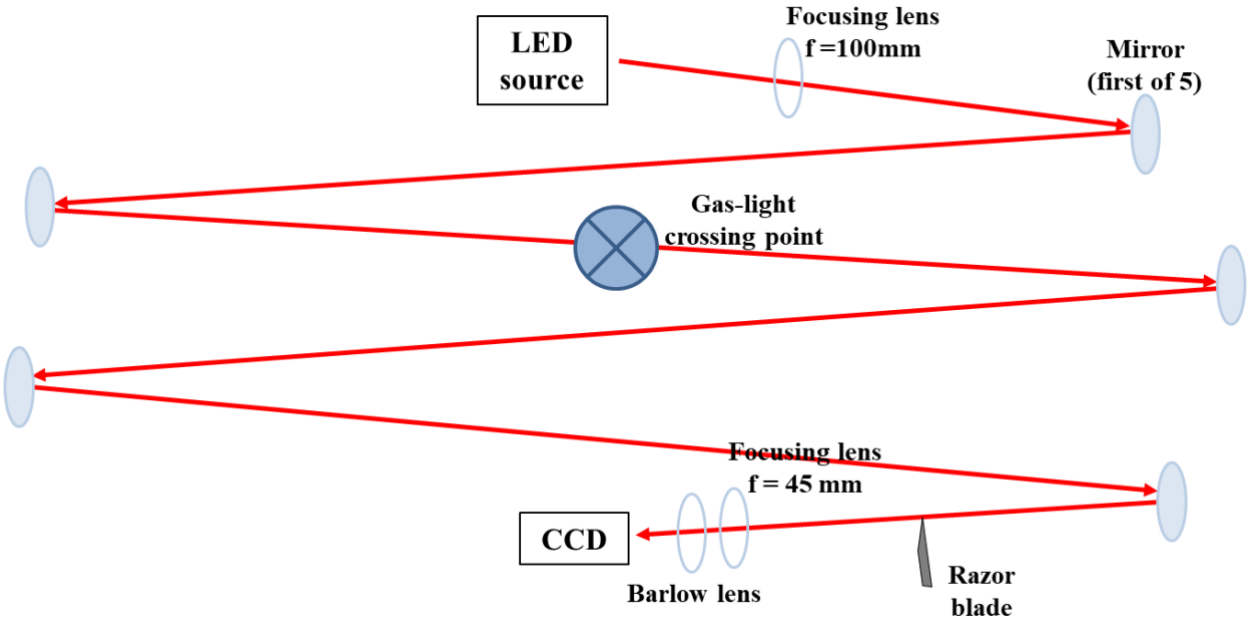
LED source
Focusing lens f =100mm
Mirror (first of 5)
Gas-light crossing point
Focusing lens f = 45 mm
CCD
Barlow lens
Razor blade

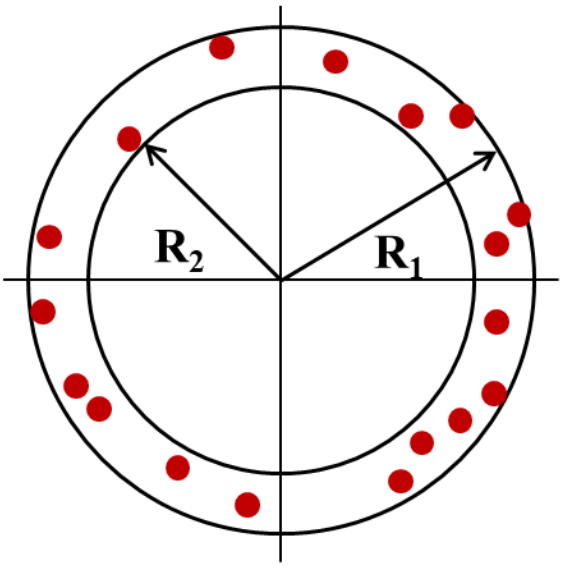
R2
R1

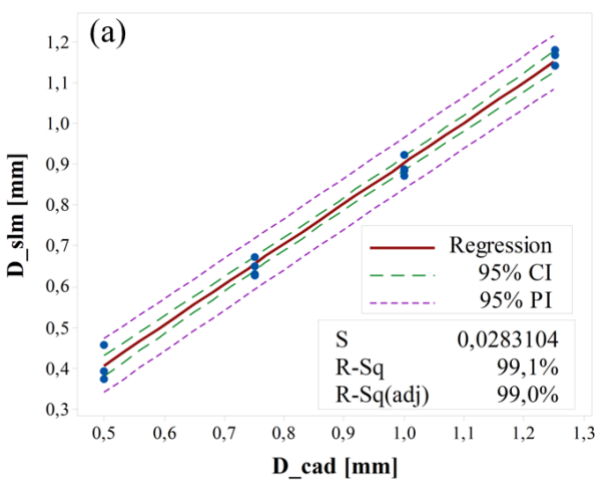
(a)
D_slm [mm]
D_cad [mm]
Regression
95% CI
95% PI
S 0,0283104
R-Sq 99,1%
R-Sq(adj) 99,0%

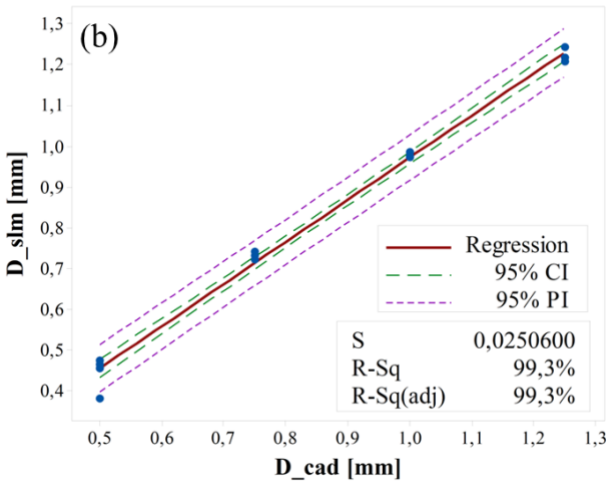
(b)
D_slm [mm]
D_cad [mm]
Regression
95% CI
95% PI
S 0,0250600
R-Sq 99,3%
R-Sq(adj) 99,3%

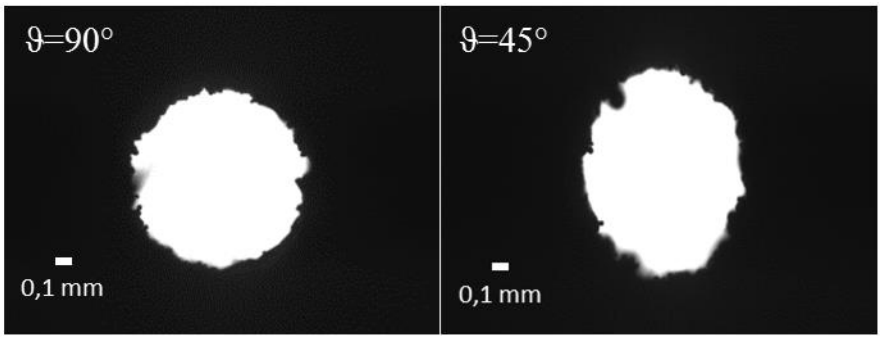
ϑ=90°
0,1 mm
ϑ=45°
0,1 mm

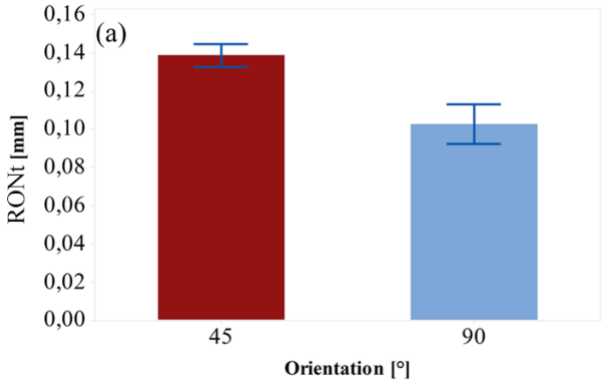
(a)
RONt [mm]
0,16
0,14
0,12
0,10
0,08
0,06
0,04
0,02
0,00
45
90
Orientation [°]

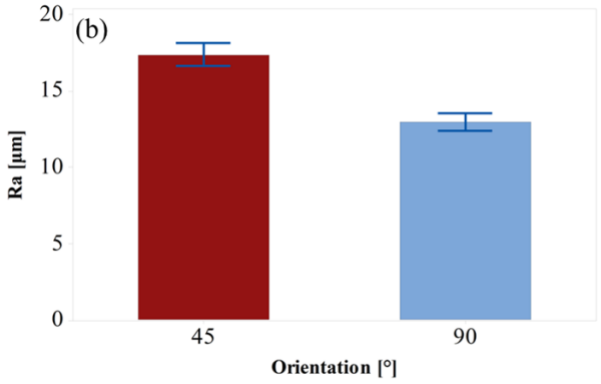
(b)
Ra [µm]
20
15
10
5
0
45
90
Orientation [°]


ϑ=90°
ϑ=45°
Build direction

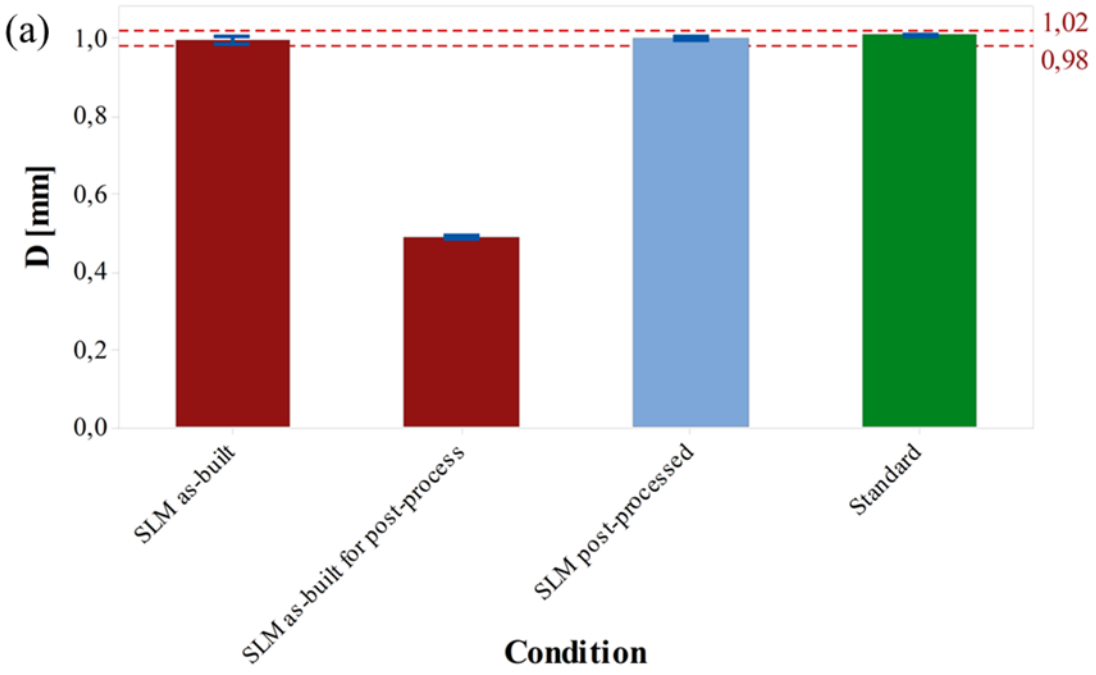
(a)
1,0
0,8
0,6
0,4
0,2
0,0
D [mm]
1,02
0,98
SLM as-built
SLM as-built for post-process
SLM post-processed
Standard
Condition

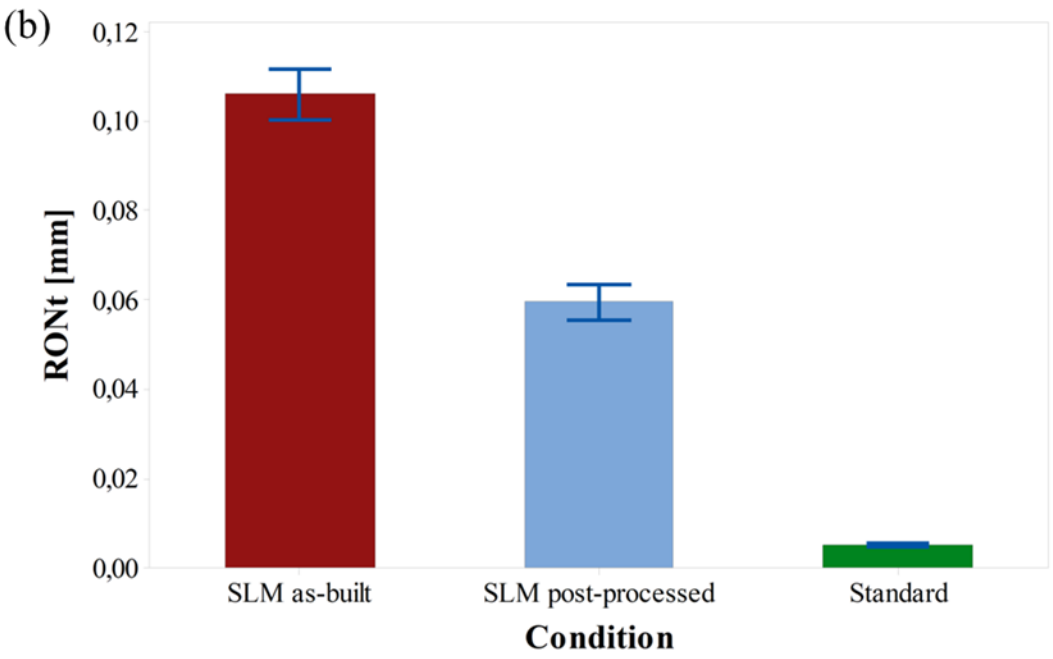
(b)
0,12
0,10
0,08
0,06
0,04
0,02
0,00
RONt [mm]
SLM as-built
SLM post-processed
Standard
Condition

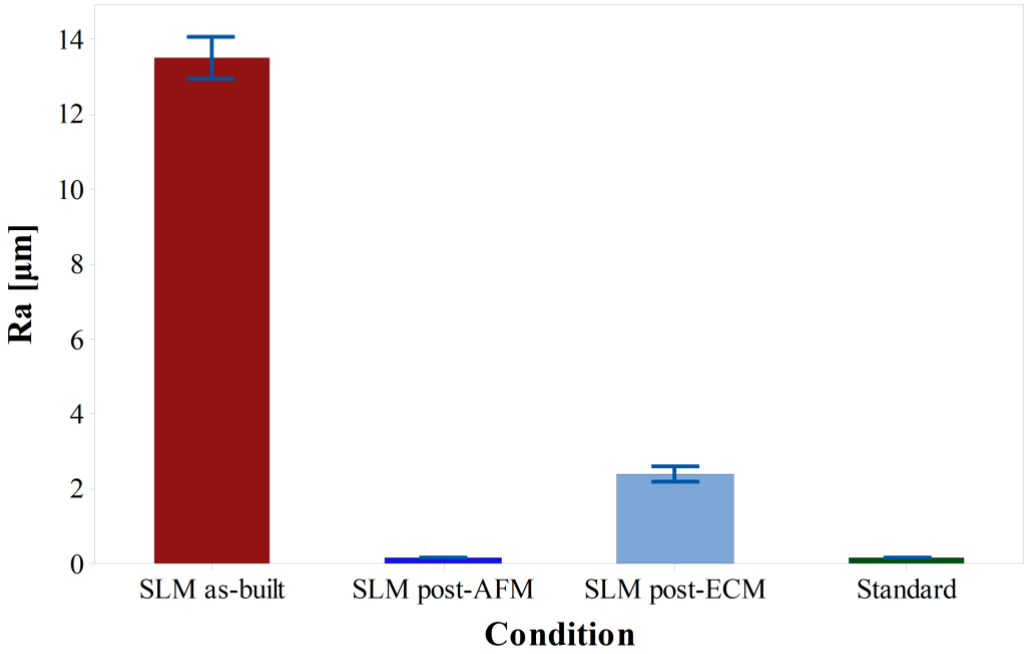
14
12
10
8
6
4
2
0
Ra [µm]
SLM as-built
SLM post-AFM
SLM post-ECM
Standard
Condition

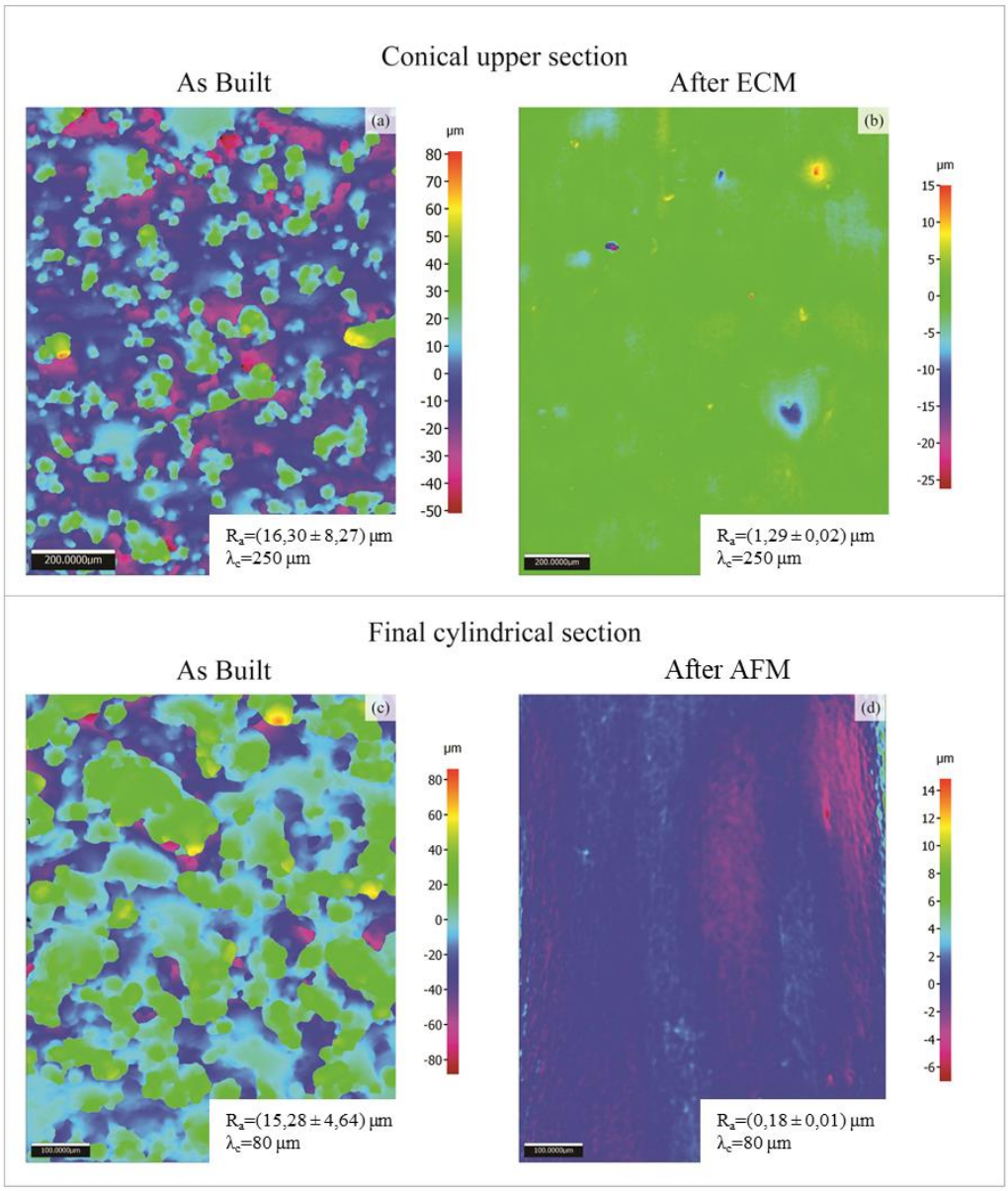
Conical upper section
As Built
After ECM
(a)
(b)
µm
80
70
60
50
40
30
20
10
0
-10
-20
-30
-40
-50
15
10
5
0
-5
-10
-15
-20
-25
200.0000µm
R_a=(16,30 ± 8,27) µm
λ_c=250 µm
R_a=(1,29 ± 0,02) µm
λ_c=250 µm
Final cylindrical section
As Built
After AFM
(c)
(d)
80
60
40
20
0
-20
-40
-60
-80
14
12
10
8
6
4
2
0
-2
-4
-6
100.0000µm
R_a=(15,28 ± 4,64) µm
λ_c=80 µm
R_a=(0,18 ± 0,01) µm
λ_c=80 µm

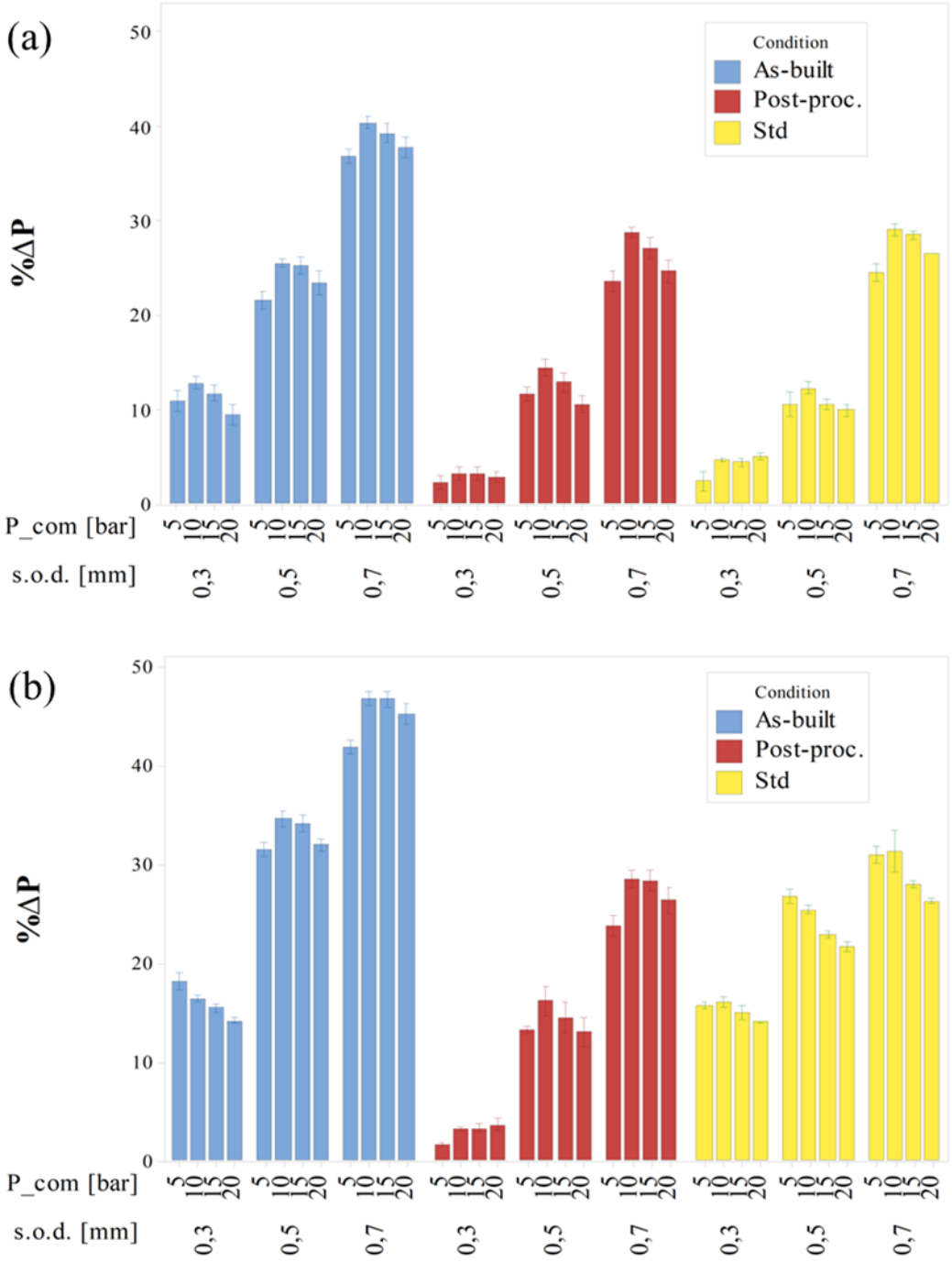
(a)
%ΔP
50
40
30
20
10
0
Condition
As-built
Post-proc.
Std
P_com [bar]
5 10 15 20
s.o.d. [mm]
0,3
0,5
0,7
(b)
%ΔP
50
40
30
20
10
0
Condition
As-built
Post-proc.
Std
P_com [bar]
5 10 15 20
s.o.d. [mm]
0,3
0,5
0,7

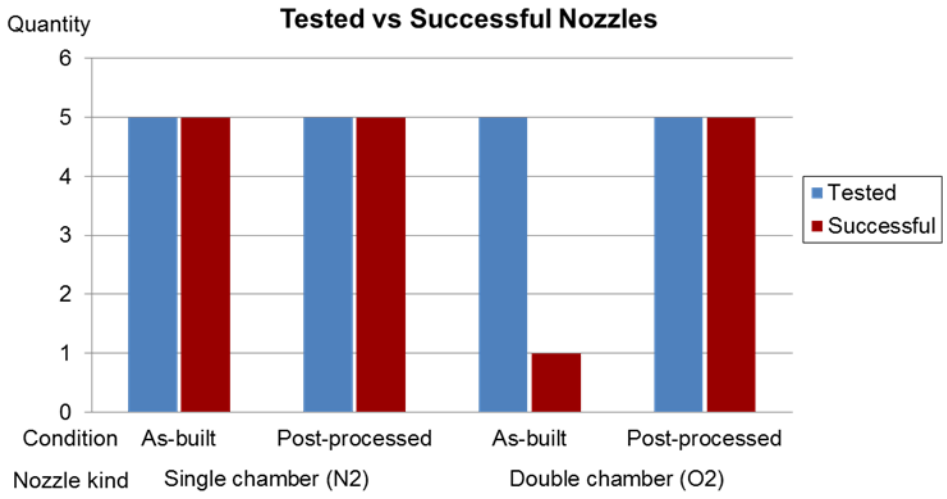
Tested vs Successful Nozzles
Quantity
6
5
4
3
2
1
0
Tested
Successful
Condition
As-built
Post-processed
As-built
Post-processed
Nozzle kind
Single chamber (N2)
Double chamber (O2)

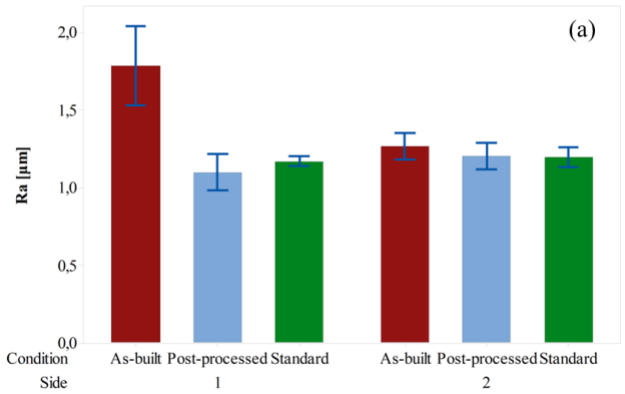
(a)
Ra [µm]
2,0
1,5
1,0
0,5
0,0
Condition
As-built
Post-processed
Standard
As-built
Post-processed
Standard
Side
1
2

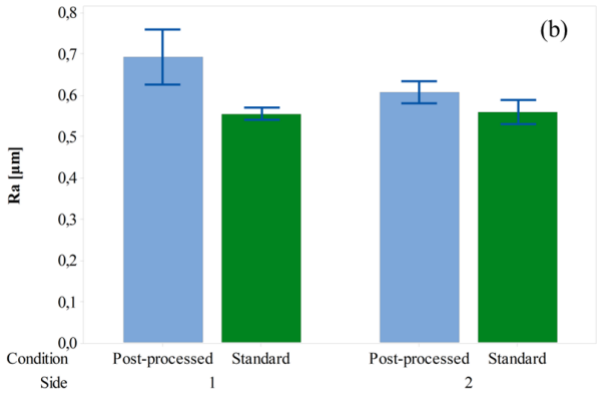
(b)
Ra [µm]
0,8
0,7
0,6
0,5
0,4
0,3
0,2
0,1
0,0
Condition
Post-processed
Standard
Post-processed
Standard
Side
1
2

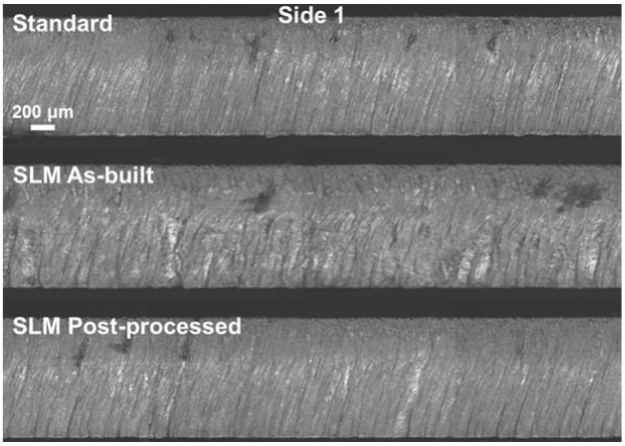
Standard
Side 1
200 µm
SLM As-built
SLM Post-processed

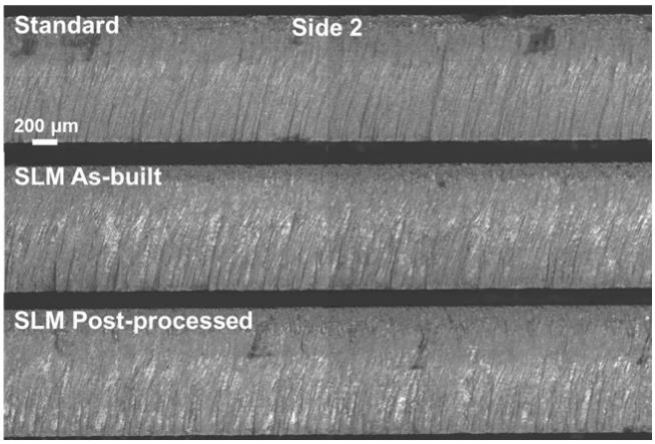
Standard
Side 2
200 µm
SLM As-built
SLM Post-processed

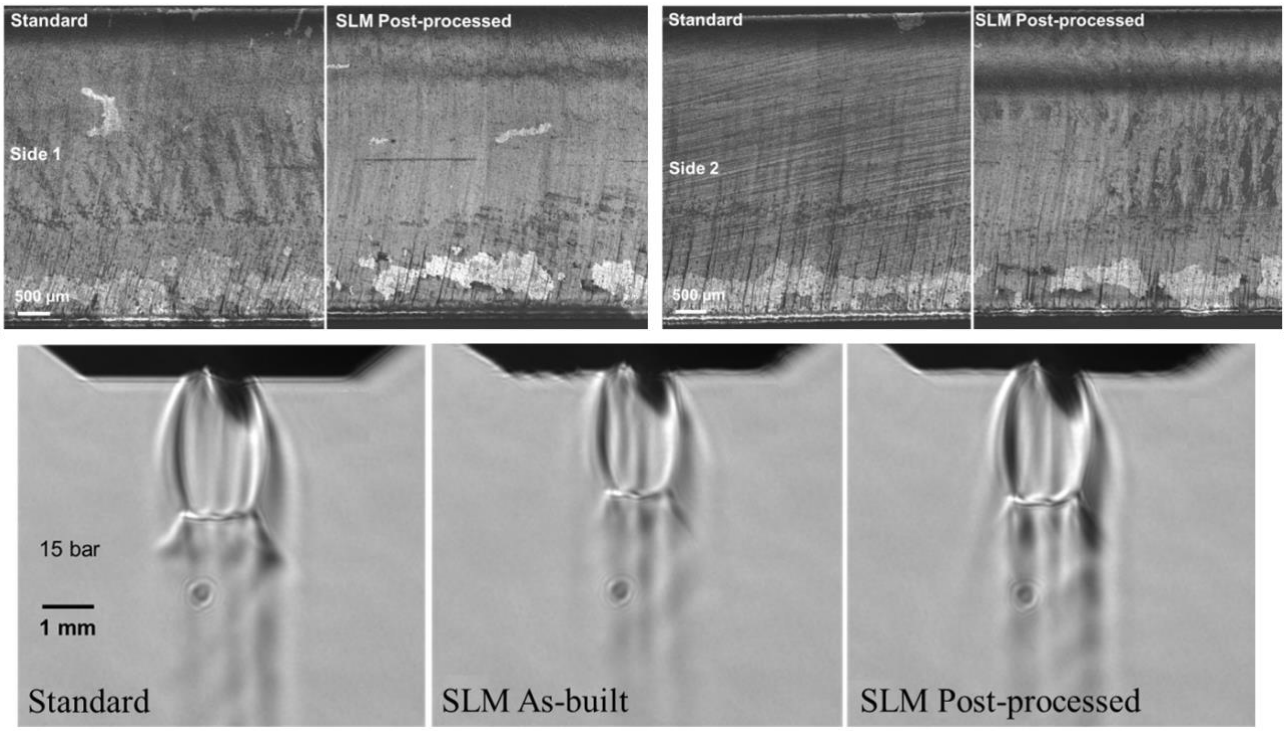
Standard
SLM Post-processed
Side 1
500 µm
Standard
SLM Post-processed
Side 2
500 µm
15 bar
1 mm
Standard
SLM As-built
SLM Post-processed